

## Article

# Enhanced Gypsum Boards with Activated Carbon Composites and Phase Change Materials for Advanced Thermal Energy Storage and Electromagnetic Interference Shielding Properties

Christina Gioti <sup>1</sup>, Konstantinos C. Vasilopoulos <sup>1,2</sup> , Maria Baikousi <sup>1,\*</sup> , Constantinos E. Salmas <sup>1</sup> , Angelos Ntaflou <sup>1</sup> , Alkiviadis S. Paipetis <sup>1</sup> , Zacharias Viskadourakis <sup>2</sup> , Rabia Ikram <sup>3</sup> , Simeon Agathopoulos <sup>1</sup>, George Kenanakis <sup>2</sup>  and Michael A. Karakassides <sup>1,\*</sup> 

<sup>1</sup> Department of Materials Science and Engineering, University of Ioannina, GR-451 10 Ioannina, Greece; christina.a.gioti@gmail.com (C.G.); kovasil@auth.gr (K.C.V.); ksalmas@uoi.gr (C.E.S.); a.ntaflos@uoi.gr (A.N.); paipetis@uoi.gr (A.S.P.); sagat@uoi.gr (S.A.)

<sup>2</sup> Institute of Electronic Structure and Laser, Foundation for Research and Technology-Hellas, N. Plastira 100, Vasilika Vouton, GR-700 13 Heraklion-Crete, Greece; zach@iesl.forth.gr (Z.V.); gkenanak@iesl.forth.gr (G.K.)

<sup>3</sup> Centre of Advanced Materials, Department of Mechanical Engineering, Universiti Malaya, Kuala Lumpur 50603, Malaysia; raab@um.edu.my

\* Correspondence: mbaikou@uoi.gr (M.B.); mkarakas@uoi.gr (M.A.K.); Tel.: +30-26510-007412 (M.B.); Tel.: +30-2651-00-7276 (M.A.K.)

**Abstract:** This work presents the development of novel gypsum board composites for advanced thermal energy storage (TES) and electromagnetic interference (EMI) shielding applications. Activated carbon (AC) derived from spent coffee with a high surface area ( $S_{\text{BET}} = 1372 \text{ m}^2/\text{g}$ ) was used as a shape stabilizer, while the commercial paraffin, RT18HC, was used as organic encapsulant phase change material (PCM). The AC showed a remarkable encapsulation efficiency as a shape stabilizer for PCM, with ~120.9 wt% (RT18HC), while the melting enthalpy ( $\Delta H_m$ ) of the shape-stabilized PCM was 117.3 J/g. The performance of this PCM/carbon nanocomposite as a thermal energy storage material was examined by incorporating it into building components, such as gypsum wallboards. The microstructure of these advanced panels, their density, and their dispersion of additives were examined using X-ray microtomography. Their thermal-regulated performance was measured through a self-designed room model with a similar homemade environmental chamber that was able to create a uniform temperature environment, surrounding the test room during heating and cooling. The measurements showed that the advanced panels reduce temperature fluctuations and the indoor temperature of the room model, in comparison with normal gypsum panels, by a range of 2–5%. The investigated gypsum board composite samples showed efficient electromagnetic shielding performance in a frequency range of 3.5–7.0 GHz, reaching an EMI value of ~12.5 dB, which is adequate and required for commercial applications, when filled with PCMs.

**Keywords:** activated carbon composites; phase change materials; gypsum boards; thermal energy storage; electromagnetic interference shielding; sustainable construction materials; RTH18C



**Citation:** Gioti, C.; Vasilopoulos, K.C.; Baikousi, M.; Salmas, C.E.; Ntaflou, A.; Paipetis, A.S.; Viskadourakis, Z.; Ikram, R.; Agathopoulos, S.; Kenanakis, G.; et al. Enhanced Gypsum Boards with Activated Carbon Composites and Phase Change Materials for Advanced Thermal Energy Storage and Electromagnetic Interference Shielding Properties. *Micro* **2024**, *4*, 61–79. <https://doi.org/10.3390/micro4010005>

Academic Editor: Hiroshi Furuta

Received: 20 December 2023

Revised: 12 January 2024

Accepted: 19 January 2024

Published: 24 January 2024



**Copyright:** © 2024 by the authors. Licensee MDPI, Basel, Switzerland. This article is an open access article distributed under the terms and conditions of the Creative Commons Attribution (CC BY) license (<https://creativecommons.org/licenses/by/4.0/>).

## 1. Introduction

In recent years, the drive towards energy storage and electromagnetic interference (EMI) shielding-efficient construction materials has led to significant advancements in the field of building science. A significant portion of energy consumption in residential areas is linked to heating and cooling needs [1]. Consequently, there is an immediate need to introduce measures focused on enhancing the energy efficiency of buildings [2]. In addition, the rapid evolution of electronic devices has generated increased worry regarding electromagnetic radiation, since it does not only possess the capability to disrupt the normal operations of devices but also pose a potential threat to human health [3].

Effectively managing electromagnetic pollution requires the development of materials aimed at electromagnetic interference shielding [4]. Researchers and engineers are continuously looking for innovative approaches to enhance the thermal performance and functional capabilities of construction materials, aiming to create structures that are not only energy-efficient but also capable of providing additional functionalities to meet the evolving demands of modern living environments [1,2,4,5]. In this context, the integration of advanced materials with multiple properties has emerged as a promising avenue for achieving such multifunctionality.

Using phase change materials (PCMs) in buildings prevents rapid changes in the inside temperature and saves energy by reducing heating/cooling demands [6–8]. PCMs possess the ability to store and release thermal energy during phase transitions, presenting an opportunity to improve indoor temperature regulation [9]. Nevertheless, the practical application of PCMs has been hindered by their inherent limitations, including low thermal conductivity and the potential issue of leakage during the phase transition when they are in the melted state [10]. The most efficient approach to prevent leakage during the solid–liquid phase transition and to minimize corrosion in structural materials involves utilizing a shape stabilizer (SS) supporting matrix. This matrix encapsulates the PCM, enabling it to maintain its molten form consistently at elevated temperatures [11–13].

Carbon-based porous materials, such as carbon-based foam, expanded graphite, graphene oxide, graphene aerogel, and activated carbon, establish a promising basis for the incorporation of functional additives like PCMs [11,14–22]. These materials possess excellent mechanical properties and electrical conductivity in combination with high surface areas and interconnected pore structures, allowing for efficient PCM impregnation and enhanced thermal conductivity and EMI shielding [4]. However, the majority of these carbon materials are costly and pose challenges in synthesis. As a result, they are not economically viable for use, especially in building applications. Activated carbon, derived from cheap biomass sources (natural waste materials, such as lignocellulose materials, rice husk, corn cob, etc., and man-made waste materials like coal-derived products, wastepaper, industrial wastes, domestic wastes, etc.), is an attractive candidate for this purpose [21]. This interest stems from its significant advantages, including a high surface area, substantial adsorption capacities, non-toxicity, low cost, easy accessibility, and environmental friendliness [21]. The use of biomass not only brings economic advantages to PCM's encapsulation field, but also encourages the conversion of waste materials into valuable products [23]. According to previous studies, activated carbon derived from peat soil [24], herb fibers [25], palm kernel shell [26], cherry stones [27], dewaxed cotton [28], waste phoenix leaf [29], pine cone [30], bamboo, pine, walnut shell, and corncob [31] was used as SS for PCMs. Moreover, activated carbon derived from leather wastes [32], straw [33–36], bagasse fiber [35,37], and animal wastes [3,38] has been studied for its EMI shielding properties.

The integration of PCMs with gypsum stands out as an attractive and favored choice in building construction [5,6,23,39–46]. This preference is attributed to the inherent benefits of gypsum, including its cost-effectiveness, fire-resistant properties, aesthetic appeal, and environmental friendliness [44,45]. Furthermore, the versatility of gypsum extends to its applicability in constructing both internal and external walls, as well as ceilings [39,44]. Nevertheless, conventional gypsum boards are predominantly crafted for structural and partitioning uses, devoid of inherent features for advanced TES and shielding against EMI. The incorporation of a carbon-encapsulated PCM could enhance these properties of gypsum boards. Zhang et al. [47] formulated gypsum boards incorporating microencapsulated PCMs through the in situ polymerization of melamine–formaldehyde copolymers. The study obtained well-dispersed additives, and the gypsum boards exhibited commendable thermal stability and a high thermal capacity when 50 wt% of additives was integrated. In a separate study, Toppi et al. [48] empirically explored the thermal performance of gypsum materials blended with commercial microencapsulated PCMs. As the additive concentration increased, the gypsum material experienced a reduction in thermal conductivity but an augmentation in specific heat. Zhang et al. studied the incorporation of SiO<sub>2</sub>-encapsulated

paraffin in gypsum, showing high mechanical strength, compactness, thermal conductivity, and a good thermal regulation performance with the weight ratio of additive at 10 wt% [43]. Recently, Chen et al. studied the incorporation of PCM encapsulated with modified commercial-activated carbon in gypsum [46].

This research paper explores the innovative integration of activated carbon–PCM composites into gypsum boards to create a new class of multifunctional construction materials. The aim is to enhance their thermal energy storage characteristics while harnessing their inherent potential to mitigate electromagnetic interference—a promising strategy towards sustainable, energy-efficient, and technologically advanced building solutions. The activated carbon derived from spent coffee was used as an SS material for phase change material, RT18HC, and incorporated into gypsum boards at different w.t. loadings. The composite gypsum boards were studied for their thermal and mechanical properties, their capacity for thermal energy storage, and their electromagnetic shielding effectiveness. Furthermore, the integration of these advanced composites into gypsum boards was examined under real-world and realistic weather conditions in a self-designed environmental chamber following the approach used by Cui et al. [49], which was able to achieve a uniform temperature environment, surrounding the test room during heating and cooling. The findings of this study have the potential to revolutionize construction practices by offering a new class of building materials that pave the way for sustainable, energy-efficient, and technologically resilient infrastructures.

## 2. Materials and Methods

### 2.1. Materials

For the experimental procedure, raw material coffee wastes were used, which were taken from a café in Ioannina in Greece. Spent coffee dried at 80 °C and without further processing was afterwards used for AC production in an inert atmosphere via pyrolysis. Potassium hydroxide (KOH, 85%), purchased from Riedel-de Haen company (Darmstadt, Germany), was used as a chemical activation reagent.

For this study, a commercial paraffin, RT18HC, was used, which was acquired from Rubitherm GmbH (Berlin, Germany). The technical specifications of this phase change material involve a melting temperature range of 17–19 °C, a heat storage capacity of  $\pm 7.5\%$  260 (kJ/kg), and solid and liquid densities of 0.88 and 0.77 (kg/L) at 15 °C and 25 °C, respectively.

For the gypsum board production, gypsum as well as starch were delivered by KNAUF (Amfilochia, Greece), a world-wide company, in order for the final product to simulate the commercial.

### 2.2. Activated Carbon Production

The activated carbon production was held via the pyrolysis process of spent coffee based on our previous published work [50] with certain alterations. More specifically, initially, spent coffee was dried at 80 °C at least for 24 h, and after, an amount of the product was mixed with potassium hydroxide (KOH) in a 1:1 w.t. ratio. During the mixing procedure, distilled water was added manually and left overnight in order to help the activation factor to be diffused through the impregnation method. Afterwards, the produced sludge was heated up until it reached 650 °C for 3 h, under an inert atmosphere (nitrogen flow of 0.2 mL/min). The pyrolysis process took place in a muffle furnace mounted with a controlling atmosphere system, and the increasing temperature rate was 3 °C/min. Subsequently, the produced activated carbon was poured into an HCl solution (1 N) and stirred for 24 h, and then the liquid was filtered, and the precipitate was washed with deionized water to a neutral pH of approximately 7. Finally, the washed product was dried at 80 °C for 24 h.

### 2.3. Paraffin Encapsulation

The paraffin encapsulation was based on already published experimental routes [14], but using the commercial RT18HC. Activated carbon was dried at 110 °C for at least 12 h in

order to remove remaining water in the sample. RT18HC was heated above melting point and dissolved with absolute ethanol, and then activated carbon was added. The solution was then stirred for 4 h under vigorous stirring. Finally, the mixture was dried at 80 °C for at least 48 h. This certain experimental procedure was used for all compositions, which are listed in Table 1.

**Table 1.** Compositions of raw materials and xRT18HC@AC composites before and after encapsulation process. Where x = 0.2, 0.5, 0.8, 1, 2, and 3 refer to RT18HC/AC ratio w.t.

Sample	Before			After
	Loading (% w.t.)	AC (g)	RT18HC (g)	RT18HC/AC (g)
0.2RT18HC@AC	20	1	0.2	1.2824
0.5RT18HC@AC	50	1	0.5	1.3850
0.8RT18HC@AC	80	1	0.8	1.6530
1RT18HC@AC	100	1	1	1.9763
2RT18HC@AC	200	1	2	2.1460
3RT18HC@AC	300	1	3	3.5998

#### 2.4. Gypsum Board Production

After examining the different proportions of the xRT18HC@AC composites, the selected material was 3RT18HC@AC with the highest RT18HC content, which was scaled up for the composite gypsum board's production. Gypsum boards (GB) were prepared by mixing the composite material-encapsulated RT18HC into activated carbon (3RT18HC@AC, which will be referred as RT18HC@AC in the next lines), with gypsum powder, starch, and water in different proportions, as listed in Table 2. Different loadings, 5–30% w.t. of the RT18HC@AC additive, were prepared. Initially, all solid materials were manually mixed homogeneously, and then the water was added under vigorous agitation. The continuous mixing was held for approximately five minutes, and then the slurry was poured into a mold, resulting in gypsum board dimensions of 20 (length) × 20 (width) × 0.13 (thickness) cm. Prior to the mold break, the slurry was left for at least 24 h to dry at room temperature.

**Table 2.** Gypsum board compositions with various RT18HC@AC additive loadings (5, 10, 15, 20, and 30% w.t.).

Gypsum Board	RT18HC@AC Additive Loading (w.t. %)	RT18HC@AC Additive (g)	Gypsum (g)	Water (g)	Starch (g)
GB	0	0	550	448	28.5
GB/RT18HC@AC-5%	5	27.5	522.5	448	28.5
GB/RT18HC@AC-10%	10	55	495	448	28.5
GB/RT18HC@AC-15%	15	82.5	467.5	448	28.5
GB/RT18HC@AC-20%	20	110	440	448	28.5
GB/RT18HC@AC-30%	30	165	385	448	28.5

#### 2.5. Leaching Tests

Leaching tests were carried out to examine the ability of the composites to impregnate the RT18HC. Originally, the weight of the composites was measured, and subsequently, encapsulated RT18HC on activated carbon was placed onto filter papers at 30 °C for 8 h and then sequentially at 80 °C for 72 h. Finally, the weight was measured once more, and the filter paper was examined for possible leakages.

#### 2.6. Density Measurements

To estimate the densities of the gypsum boards, the Archimedes' immersion method was used. However, the porosity of the materials was a huge obstacle, so the modified water

displacement method was performed according to published standard [51]. According to this standard, porous gypsum samples were previously wax sealed and then immersed into a dimension measured cylinder.

### 2.7. X-ray Computed Microtomography (Micro CT)

X-ray computed microtomography (micro-CT) imaging was employed to investigate the internal structure of gypsum board reference (GB) and GB/RT18HC@AC composites with varying concentrations of additive (10%, 20%, and 30%). Radiographic imaging was carried out on a Bruker SkyScan 1275 (Billerica, MA, USA) scanner, equipped with a distortion-free 3 Mp active flat-panel detector. An accelerating voltage of 60 kV and a current of 60  $\mu$ A were applied, while a 1 mm thick Al filter was used. The object distance was 20 mm, leading to a pixel size of 10  $\mu$ m. A 360° scan was performed with a 0.20° rotation step corresponding to 25 min scan duration. The reconstruction was performed on Bruker's NRecon—v2.1.0.1 software. CTan and Dataviewer were used for the image analysis.

### 2.8. Thermogravimetric Analysis (TGA)

Thermogravimetric analysis was held through a Setsys Evolution-Setaram TG-DTA (Prague, Czech Republic) analyzer. Approximately 30 mg of the composites was placed into a platinum crucible, and then heating and gas ( $N_2$ ) flow rates were adjusted constantly for all experiments at 5  $^{\circ}C\ min^{-1}$  and 25 mL  $\min^{-1}$ , respectively, while temperature ranged from ambient to 700  $^{\circ}C$ .

### 2.9. Thermal Properties

Differential Scanning Calorimeter (DSC) measurements were carried out under  $N_2$  atmosphere using DSC 214 NETZCH Polyma instrument (Selb, Germany). Heating and cooling rate was 2  $^{\circ}C/\min$ , and temperature ranged from 0  $^{\circ}C$  to 40  $^{\circ}C$  and from 40  $^{\circ}C$  to 0  $^{\circ}C$ , respectively.

The thermal transport properties of gypsum board specimens, including thermal conductivity ( $k$ ) and heat capacity ( $C_p$ ), were assessed using a C-Therm TCi Thermal Conductivity analyzer (Fredericton, Canada). The Modified Transient Plane Source (MTPS) method (ASTM D7984) [52] was employed, wherein a one-sided thermal sensor applied a low-energy current pulse to the specimen for 0.8 s. This ensured that the measurement of thermal conductivity ( $k$ ) was not influenced by thermal convection. Some of the heat generated was absorbed by the specimens, while the remaining portion was utilized to raise the temperature at the sensor–sample interface. The resulting temperature variation indicated a resistance change in the sensor, leading to a voltage drop. The voltage data were utilized to assess the thermal transport properties of the investigated material.

Thermal conductivity ( $k$ ) and thermal effusivity ( $e$ ) were measured directly, providing a detailed overview of the heat transfer properties of the sample material. The final values were derived from an average of 5 measurements for the specimen using the polymer test method and using pyrex glass as a standard ( $k = 1.143\ W/m\cdot K$ ). The heat capacity ( $C_p$ ) was then calculated using an equation ( $C_p = e^2/k\cdot\rho$ ) where  $\rho$  is the density of each specimen.

### 2.10. Mechanical Properties

#### 2.10.1. Low-Velocity Impact Testing

For the low-velocity impact testing, an Instron Ceast 9340 Drop Tower (Norwood, MA, USA) equipped with a 45 kN loadcell and a 16 mm hemispherical impactor with a mass of 2.5 kg was used. Impact energy was selected at 2 J. Each specimen (50 mm  $\times$  50 mm  $\times$  12.5 mm) was placed onto a metallic mask with dimensions of 150 mm  $\times$  100 mm  $\times$  3 mm according to ASTM C90-15 [53], with a square gap in the center of the area ( $\sim 9\ cm^2$ ). The mechanical knockdown effect and the repair efficiency at gypsum specimens were evaluated in terms of maximum impact load (kN) and absorbed energy (J). The absorbed energy was calculated by measuring the area under the load–displacement curve. In any case, breakage of the specimens was observed; therefore, the tests can be considered as penetration tests.

### 2.10.2. Modulus of Rupture, MOR

The modulus of rupture, MOR, was determined via three-point bending strength tests (Autograph AGS-H; Shimadzu, Kyoto, Japan), according to ASTM C293/C293M-16 [54]. More specifically, the cross-sectional dimensions of each specimen were measured (the accuracy was  $\pm 0.01$  mm). Then, the gypsum specimen was centered at the gap (the span was 100 mm) between the supporting rods of the test machine. The velocity of the bending load was 2.0 mm/min, and the load until fracture was measured. The flexural strength ( $\sigma$ ) was calculated using Equation (1):

$$MOR = \frac{3WL}{2bd^2} \quad (1)$$

where  $W$  (N) is the fracture load, and  $L$ ,  $W$ , and  $h$  are the span between the supporting rods, the specimen width, and the thickness, respectively. Five specimens from each subgroup ( $n = 5$ ) were tested.

### 2.11. Thermal Performance Measurements

Thermal performance measurements were conducted using a custom-made environmental chamber [49].

The environmental chamber (Figure S1), constructed from polystyrene foam panels, featured internal dimensions measuring 1000 mm in length, 1000 mm in width, and 1000 mm in height. A fan heater and a portable air conditioner were installed through an opening in the top section of the side panel.

Beneath the environmental chamber, four smaller chambers with internal dimensions of 200 mm in length, 200 mm in width, and 200 mm in height were positioned to serve as test rooms. These chambers, constructed from polystyrene foam panels, featured a design where the top side panel was hollow, allowing for the placement of test samples.

Temperature measurements were conducted using Type K thermocouples positioned at the center of each test room, with additional thermocouples attached to both the outer and inner surfaces of every test sample. Furthermore, another thermocouple was centrally placed within the environmental chamber for comprehensive temperature monitoring.

The chamber's internal temperature was elevated and decreased by the heater and portable air conditioner, respectively, from the top of the chamber. As a result, the thermal reactions of the test samples under varying temperature conditions could be assessed.

Temperature measurements were recorded every 5 min.

### 2.12. Electromagnetic Interference (EMI) Shielding Properties

The EMI shielding effectiveness properties were evaluated using a P9372A Keysight.

A Streamline Vector Network Analyzer (Keysight, Santa Rosa, CA, USA) and two sets of microwave standard 15 dB gain waveguides were used (WR 187 and WR 147, respectively, obtained from Advanced Technical Materials Inc. (ATM), Patchogue, NY, USA), covering a broad C frequency band in the range of 3.5–7.0 GHz (C-band), which is used for long-distance radio telecommunications, such as satellite communications transmissions, Wi-Fi devices, cordless telephones, weather radar systems, etc. In particular, every sample was placed in the middle of each set of waveguides, and its scattering parameters (S-parameters; S11, S12, S22, S21) were recorded.

## 3. Results and Discussion

### 3.1. Characterization of RT18HC@AC Filler

The structural and physicochemical characterizations of the AC matrix are presented in detail in our previous work [50]. The activated carbon exhibits a microporous structure with a high surface area ( $S_{BET} = 1372 \text{ m}^2/\text{g}$ ) and pore volume ( $0.75 \text{ cm}^3/\text{g}$ ), which are properties that make it a suitable material for encapsulating PCM. The next sections present the properties of the RT18HC@AC filler concerning leaching tests and their thermal behavior.

### 3.1.1. Leaching Tests for RT18HC@AC Filler

Leaching tests were performed for the RT18HC@AC samples with different RT18HC loadings (20, 50, 80, 100, 200, and 300% w.t.) according to the procedure explained in the experimental section. Figures 1 and 2 show the filter papers after the leaching tests at 30 and 80 °C, respectively. The absence of paraffin observed on the filter papers after the leaching tests (no oily marks are apparent) is an important feature that indicates the efficacy of the RT18HC@AC composite in encapsulating and retaining the RT18HC component. This observation suggests that the composite material exhibits a high degree of stability under the specified leaching conditions and no leaching of the PCM phase.

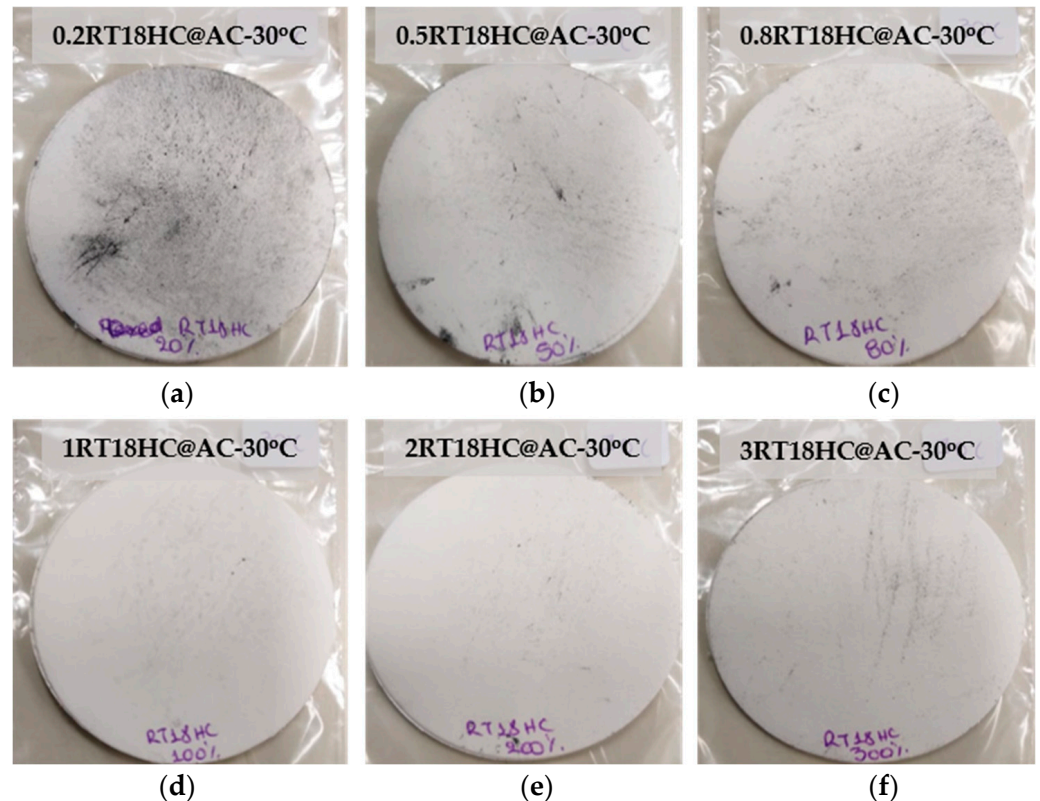
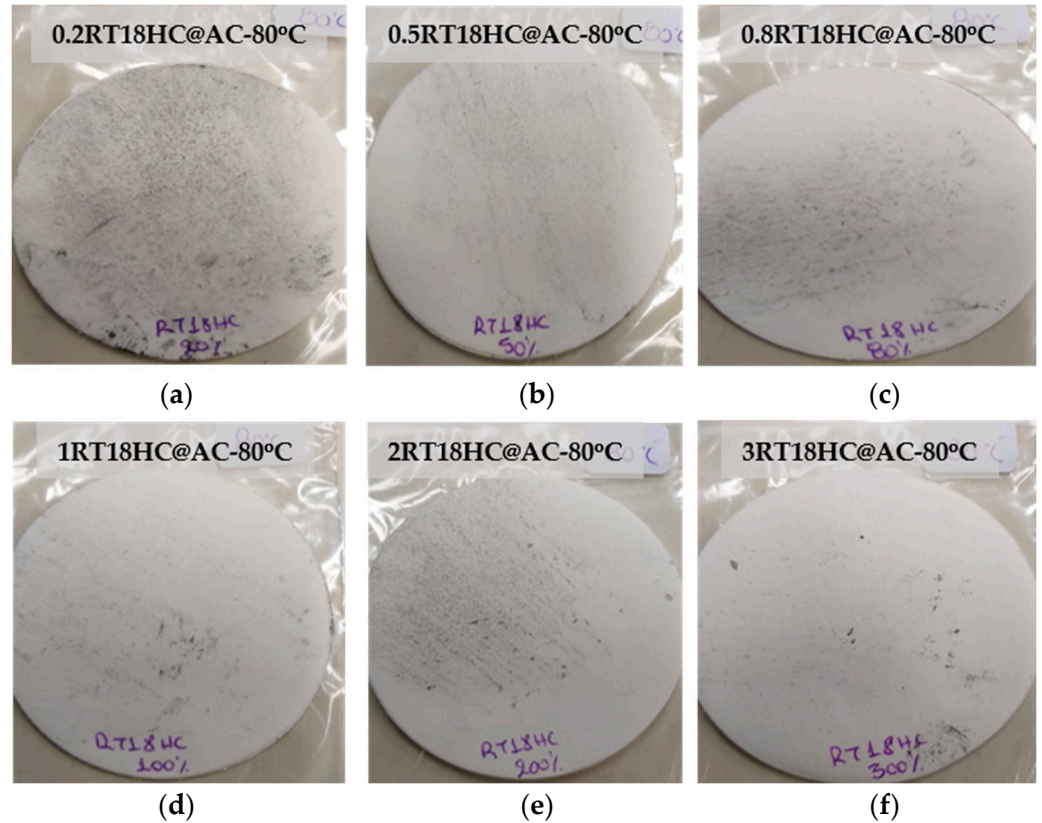


**Figure 1.** Leaching tests at 30 °C for 8 h of the produced hybrid AC-RT18HC samples with (a) 20%, (b) 50%, (c) 80%, (d) 100%, (e) 200%, and (f) 300% RTHC18.

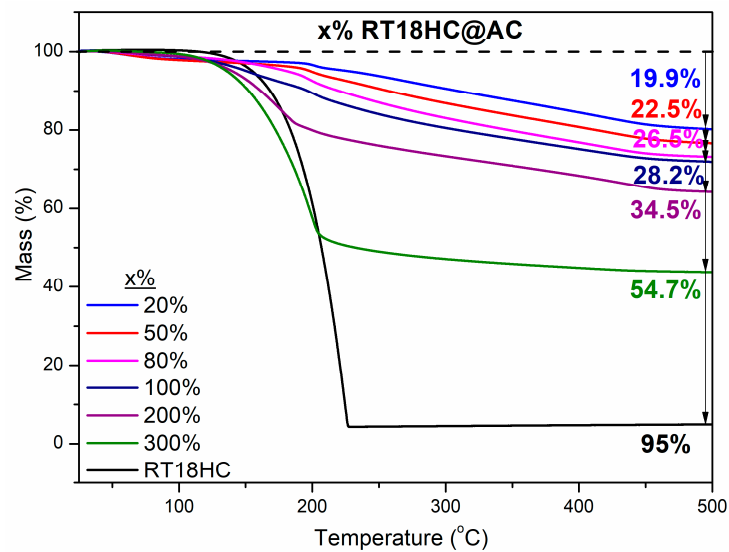
### 3.1.2. Thermal Properties of AC-RT18HC Filler

A thermogravimetric analysis (TGA) was employed to study the thermal degradation characteristics of the RT18HC@AC composites, with different RT18HC loadings, as well as to estimate the real mass of RT18HC encapsulation into the activated carbon matrix. Figure 3 presents the TG% curves of the composite materials in comparison with pure RT18HC. The TG% curve of pure RT18HC reveals one thermal degradation stage at the range of ~130–230 °C, which is accompanied with a 95% weight loss due to the volatilizations of paraffin. In the case of the RT18HC@AC composites, a noteworthy trend emerged as a function of RT18HC loading, wherein an increase in the RT18HC content was correlated with a higher mass loss from 19.93% for a 10% loading to 54.73% for 300% loading. Also, RT18HC thermal degradation occurred at two stages, one at a temperature up to 230 °C, and a second one at higher temperatures up to 460 °C. The initial weight loss, which is observed at lower temperatures, probably corresponds to the thermal degradation of RT18HC, which is adsorbed on the outer surface of activated carbon (macropores), whereas the second weight loss at higher temperatures is attributed to same degradation of the RT18HC molecules that are adsorbed on the smaller meso- and micropores where more energy is needed for their degradation. Table 3 summarizes RT18HC loading on AC according to weighting

and thermogravimetric results. The 3RT18HC@AC material was selected as the additive for the composite gypsum boards since it exhibits the higher PCM loading (54.73%), and no leaching of the PCM phase was observed during the leaching tests. Although none of the xRT18HC@AC materials showed leaching of the PCM component, the materials with the highest PCM loadings on AC are preferable since they will offer more encapsulated effective materials on the gypsum board, leading to better thermal storage properties.



**Figure 2.** Leaching tests at 80 °C for 72 h of the produced hybrid AC-RT18HC samples with (a) 20%, (b) 50%, (c) 80%, (d) 100%, (e) 200%, and (f) 300% RTHC18.

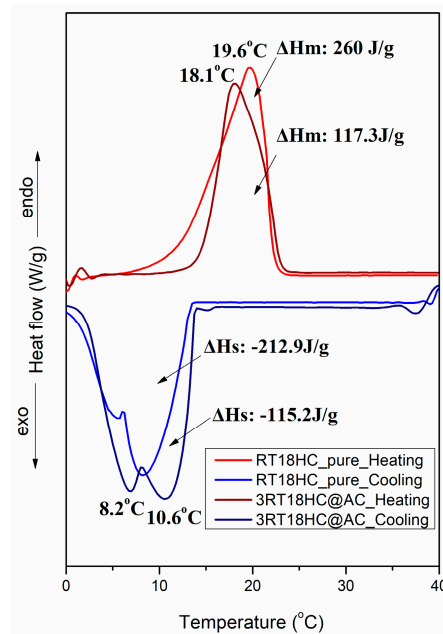


**Figure 3.** Thermogravimetric analysis (TG%) curves of AC-RT18HC hybrids with different RTHC18 loading during the synthesis.

**Table 3.** RT18HC loading on AC according to weighting and thermogravimetric results.

Sample	Initial Loading (% w.t.)	Weighting Increment (% w.t.)	Mass Loss on TG Curves (% w.t.)	Encapsulation According to TG Curves (% w.t.)
0.2RT18HC@AC	20	28.24	19.93	24.90
0.5RT18HC@AC	50	38.50	22.48	29.00
0.8RT18HC@AC	80	65.30	26.47	36.00
1RT18HC@AC	100	97.63	28.24	35.80
2RT18HC@AC	200	114.60	34.46	52.60
3RT18HC@AC	300	260.00	54.73	120.90

Figure 4 shows the DSC curves of the 3RT18HC@AC composite in comparison with the corresponding curves of pure RT18HC. Also, the melting and freezing temperatures ( $T_m$  and  $T_s$ ) as well as the corresponding enthalpies ( $\Delta H_m$  and  $\Delta H_s$ ) are shown in this figure. The melting point of pure RT18HC at 19.6 °C and its freezing point at 8.2 °C align with its known phase change characteristics. The observed asymmetry in the exothermic and endothermic peaks suggests the presence of multiple crystalline phases within RT18HC. According to the Rubitherm data sheet [55], the RT18HC's structure appears to consist of multiple hydrocarbons, with hexadecane ( $C_{16}H_{34}$ ) being identified as the primary component. This complexity in composition and structure can lead to varied energy requirements for melting and freezing, resulting in the observed asymmetry in the thermal response. In the case of the 3RTHC18@AC composite, the encapsulated RT18HC melts at a lower temperature, at 18.1 °C (−1.5 °C), and freezes at higher temperature, at 10.6 °C (+2.4 °C). The corresponding enthalpies of pure RT18HC and RT18HC encapsulated on activated carbon were calculated using the areas under the exothermic (melting) and endothermic (solidification) transition peaks in their respective DSC curves. The results revealed enthalpies of 260.0 J/g ( $\Delta H_m$ ) and −212.9 J/g ( $\Delta H_s$ ) for pure RT18HC and enthalpies of 117.3 J/g ( $\Delta H_m$ ) and −115.2 J/g ( $\Delta H_s$ ) for the encapsulated RT18HC.

**Figure 4.** DSC curves of 3RT18HC@AC composite in comparison with the corresponding curves of pure RT18HC.

The theoretical melting enthalpy of the composite material was calculated using the following equation [56]:

$$\Delta H_m^{theoretical} = \Delta H_m^{PCM}(1 - \varphi\%) \quad (2)$$

where  $\Delta H_m^{theoretical}$  and  $\Delta H_m^{PCM}$  are the theoretical melting enthalpy of the 3RT18HC@AC composite and the measured melting enthalpy of RT18HC, respectively, and  $\varphi\%$  is the weight fraction of the sample. Using the above equation, the theoretical melting and freezing enthalpies of 3RT18HC@AC were found to be 117.78 J/g and 96.44 J/g, respectively, for a 54.7% RT18HC content, according to the thermogravimetric analysis. These values seem consistent with the values measured using DSC (117.3 and  $-115.2$  J/g, respectively).

### 3.2. Characterization of Gypsum/RT18HC@AC Composite Boards

#### 3.2.1. Density and Microtomography Results for GB/RT18HC@AC Composite Boards

Figure 5 displays the images of the reference gypsum board (GB) and the GB/RT18HC@AC composite boards. The results of the density measurements are presented in Table S1, and the plotted versus % w.t. content of 3RT18HC@AC are shown in Figure 6. The density results reveal a systematic reduction in the density of gypsum boards with an increase in the RT18HC@AC additive content. The reduction in density is attributed to the incorporation of the RT18HC@AC additive, which introduces lightweight particles into the matrix of the gypsum. Despite the reduction in composite densities with an increasing additive content, all composites still meet the minimum density requirement of  $0.60 \text{ g cm}^{-3}$  set by the European regulation UNE-EN 13279-1 for gypsum binders and gypsum plasters [57,58].

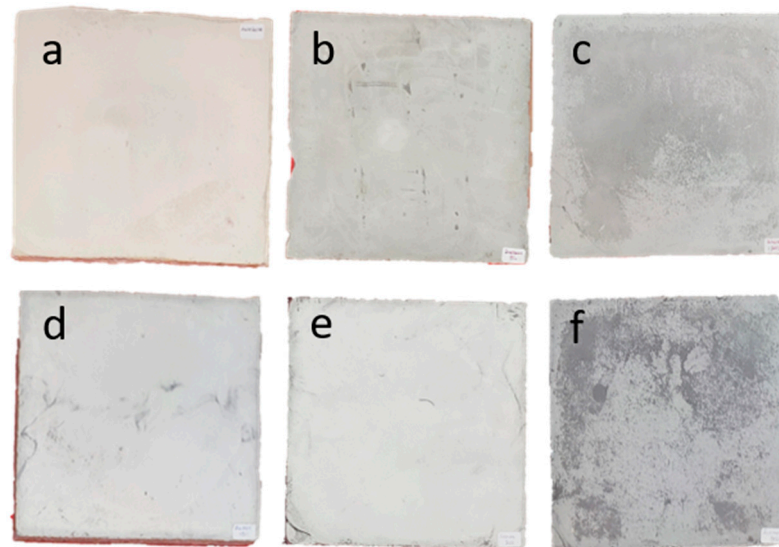


**Figure 5.** (a) Reference gypsum board (GB) and GB/RT18HC@AC composite boards ( $200 \times 200 \times 12.5$  mm) with (b) 5, (c) 10, (d) 15, (e) 20, and (f) 30% w.t. RT18HC@AC.

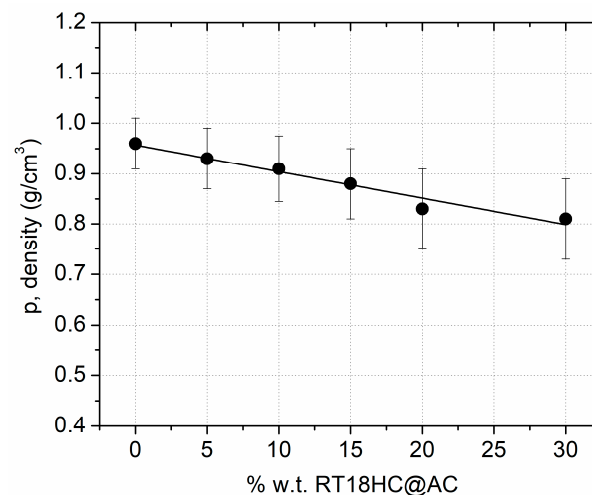


**Figure 6.** Graphical plot of GB/RT18HC@AC density versus % w.t. content of RT18HC@AC additive.

To validate the findings and examine the structure of the gypsum, X-ray computed microtomography ( $\mu$ CT) was performed. These results provide critical insights into the relationship between the additive concentration and the microstructural characteristics of the composites. The microscale images (Figure 7) reveal distinctive features corresponding to the different levels of additive incorporation. The colored scale bar in the images refers to the different X-ray attenuation values, and as a result, the different physical density values of the gypsum board components, beginning from the lower index (black) to the higher index (white). The black spots in all images correspond to the lower intensity areas (air voids), which are the porous areas of the boards. In the case of the GB reference board, the images mainly consist of green- and yellow-colored areas. At a 10% additive concentration, the microtomography images show initial alterations in the material's density, with obvious differences in the RT18HC@AC particle distribution. The images exhibit less green and yellow areas, while new red and purple areas (lower index components) appear. The last probably corresponds to RT18HC@AC particles, which are observed to be homogeneously integrated into the gypsum matrix, marking the beginning of structural modifications. When increasing the additive concentration to 20% and 30%, these lower index areas (red and purple coloured) become more intense, resulting in a more pronounced impact on the internal architecture. The microtomography images demonstrated an enhanced homogeneity in RT18HC@AC dispersion, even at the board with 30% additive, indicating a uniform integration within the gypsum matrix.

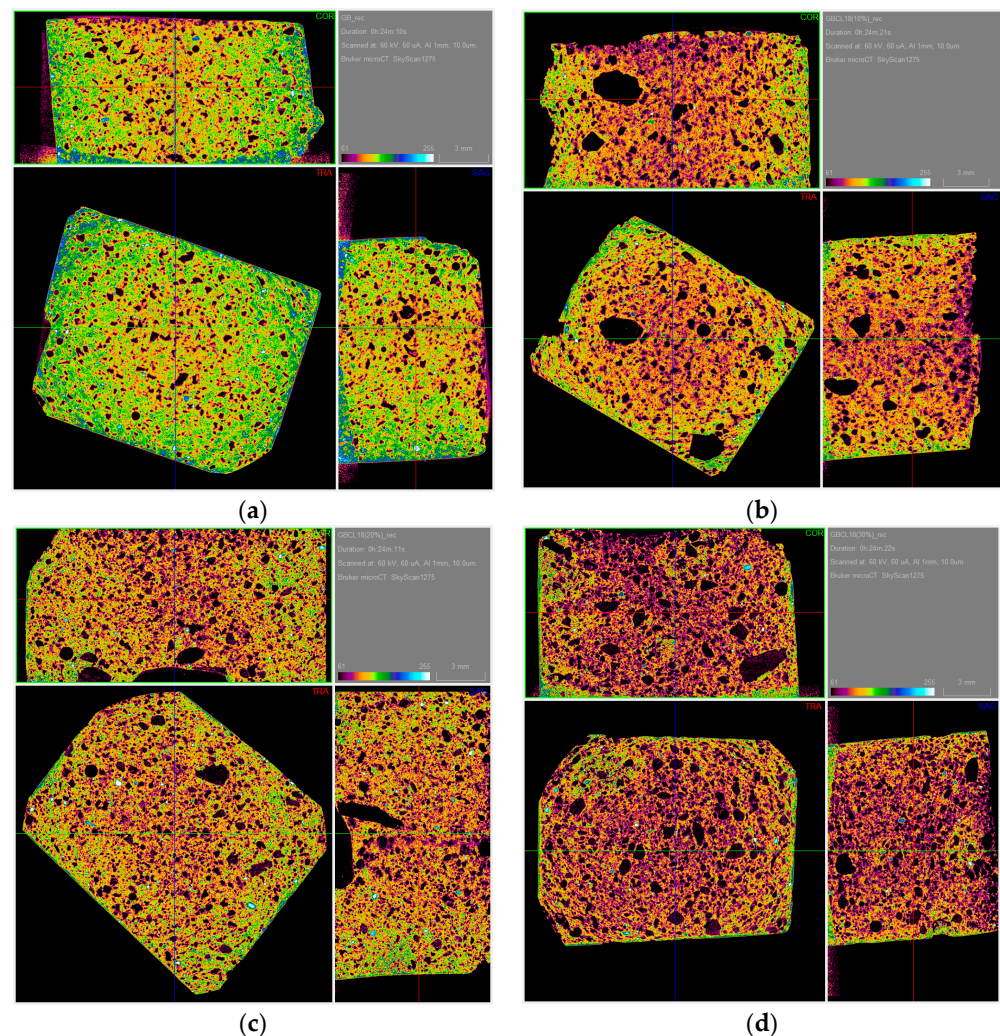


**Figure 7.** X-ray computed microtomography (micro CT) results from GB (a) and GB/RT18HC@AC boards with 10% (b), 20% (c), and 30% (d) additive content.

### 3.2.2. Thermal Properties of GB/RT18HC@AC Composite Boards

The results of the thermal conductivity and specific heat capacity measurements for the reference gypsum board and composite GB/RT18HC@AC gypsum board with varying RT18HC@AC contents are summarized in Table S2. Also, Figure 8 presents the graphical correlation of the thermal conductivity ( $k$ ) and specific heat capacity ( $C_p$ ) with the increase in percentage content of RT18HC@AC additive. As depicted in the data, an incremental rise in the percentage content of additive corresponds to noticeable variations in these parameters. Particularly, a positive correlation is observed, signifying an enhancement in the thermal conductivity and specific heat capacity with a higher additive content. This positive relationship is interpreted as the positive contribution of the RT18HC@AC component to the heat transfer capabilities within the composite gypsum boards.

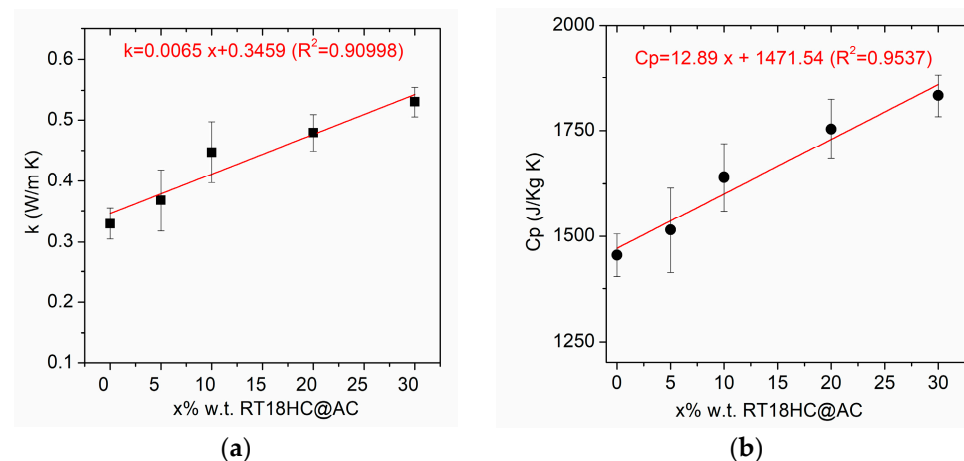


**Figure 8.** Graphical plot of GB/RT18HC@AC. (a) Thermal conductivity,  $k$ , and (b) specific heat capacity,  $C_p$ , versus % w.t. content of RT18HC@AC additive.

### 3.2.3. Mechanical Properties of GB/RT18HC@AC Composite Boards

The results of the mechanical properties from the bending and impact resistance tests for the gypsum board and composite GB/RT18HC@AC board with varying RT18HC@AC contents are shown in Figures 9 and 10, respectively. The load deformation data reveal a complex relationship between the percentage of additive and the mechanical behavior of the composite boards. At lower concentrations, a positive correlation is evident, suggesting that the incorporation of RT18HC@AC enhances the material's strength, which is possibly due to improved intermolecular interactions and reinforcement effects. However, as the RT18HC@AC content increases, a decline in the mechanical strength is observed. This inverse relationship could be attributed to the potential disruption of the gypsum matrix by higher concentrations of RT18HC@AC particles. As it shown in Figure 9b, the optimal content of the additive onto gypsum boards is 10% w.t., showing that the modulus of rupture is equal to 4.68 MPa, which is much higher than that of the reference gypsum board (2.64 MPa).

The data from the impact resistance tests also show a similar trend (Figures S2 and 10, Table S3). An analysis of the data in Table S3 reveals that the presence of RT18HC@AC additive in the gypsum boards leads to an increase in both the maximum load ( $F_{max}$ ) and absorbed energy ( $E_a$ ) when compared to the reference GB sample. This increase is subtle and remains consistent up to approximately a 20% w.t. additive content. However, for higher percentages of additive, a notable mechanical degradation becomes apparent. However, in this case, too, the optimal content of the additive in gypsum boards is 10% w.t., showing the highest values for  $F_{max}$  (960.07 N) and  $E_a$  (1.709 J), which are much higher than those of the reference gypsum board (605.84 N and 1.632 J, respectively).

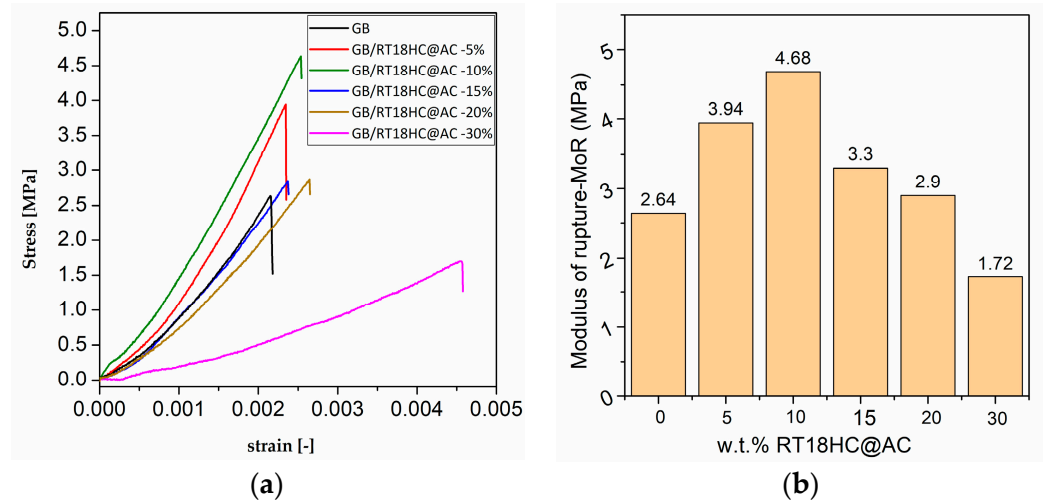


**Figure 9.** Results from the bending tests. (a) Stress–strain curves and (b) the modulus of rupture for the gypsum boards with varying % w.t. contents of RT18HC@AC additive.

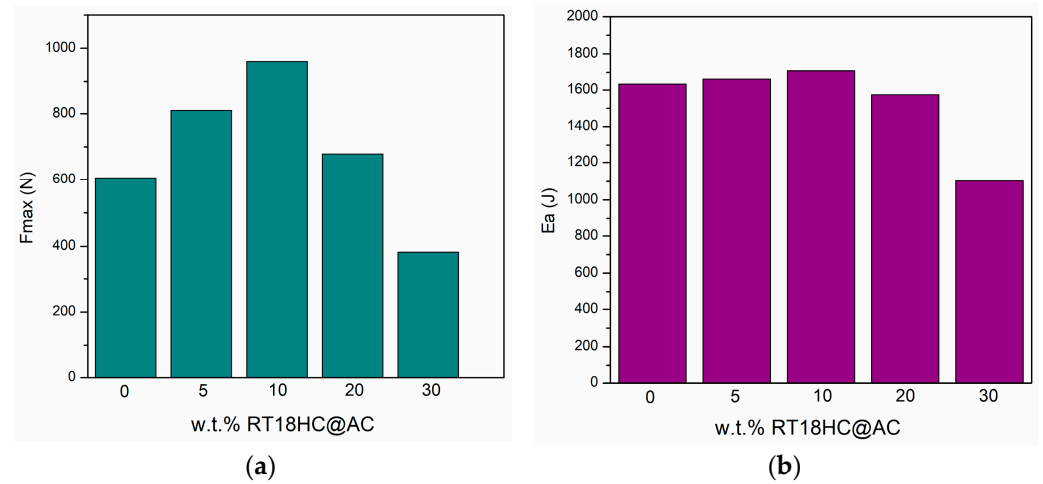


**Figure 10.** Results from the impact resistance tests. (a) Maximum load,  $F_{max}$ , and (b) absorbed energy,  $E_a$ , for the gypsum boards with varying % w.t. contents of RT18HC@AC additive.

### 3.2.4. EMI Shielding Properties for GB/RT18HC@AC Composite Boards

The performance of the EMI protection of developed samples was assessed from the point of view of the EMI protection ( $SE$ ) efficiency in the frequency range of 3.2–7.0 GHz. Electromagnetic shielding literally means that when an electromagnetic field occurs in a system enclosed in a shield material, there is a minimum or ideally absent transmission over the shield material and in the system.

$SE_T$  can be expressed as the sum of reflection from the surface ( $SE_R$ ), absorption ( $SE_A$ ), and multiple reflection ( $SE_M$ ) as follows [59]:

$$SE_T(\text{dB}) = SE_R(\text{dB}) + SE_A(\text{dB}) + SE_M(\text{dB}) \quad (3)$$

Generally, multiple reflection at internal interfaces inside the material can be excluded if  $SE > 10\text{--}15$  dB [59–61]. Thus, we calculated the average  $SE_T$  as

$$SE = SE_T \triangleq 10 \log_{10} \left( \frac{P_{inc}}{P_{trn}} \right) = 10 \log_{10} \left( \frac{1}{T} \right) = SE_R + SE_A \quad (4)$$

where

$$SE_R = 10 \log_{10} \left( \frac{1}{1 - R} \right) \quad (5)$$

$$SE_A = 10 \log_{10} \left( \frac{1 - R}{T} \right) \quad (6)$$

$SE_R$  and  $SE_A$  refer to the reflection and absorption SE, respectively.

The higher the SE, the better the shielding. The SE (also denoted as  $SE_T$ , with  $A$ ,  $T$ , and  $R$  indicating the absorption, transmission, and reflection, respectively) is usually quantified in terms of the logarithm of the incident power  $P_{inc}$  over the transmitted power  $P_{trn}$  [62–65] and is thus expressed in decibels (dB).

Figure 11 depicts the absorption (Figure 11a) and the reflection (Figure 11b) spectra of the GB/RT18HC@AC composite samples for a series of additive RT18HC@AC concentrations in the frequency range of 3.5–7.0 GHz. Figure 11b clearly illustrates that the reflection of the samples is almost zero for all of the additive concentrations from 0.00 to 30% w.t. As a result, the EMI shielding effect due to reflection ( $SE_R$ ) is also negligible (see Figure 11d), and in all cases, the total SE is simply  $SE_T = SE_A$  (see Equation (4)), which is in agreement with the results of other research groups working on carbon allotropes [66]. Clearly, the dominant shielding mechanism is absorption, which is also supported by the continuously increasing absorption levels with an increasing RT18HC@AC content in the gypsum board composites.

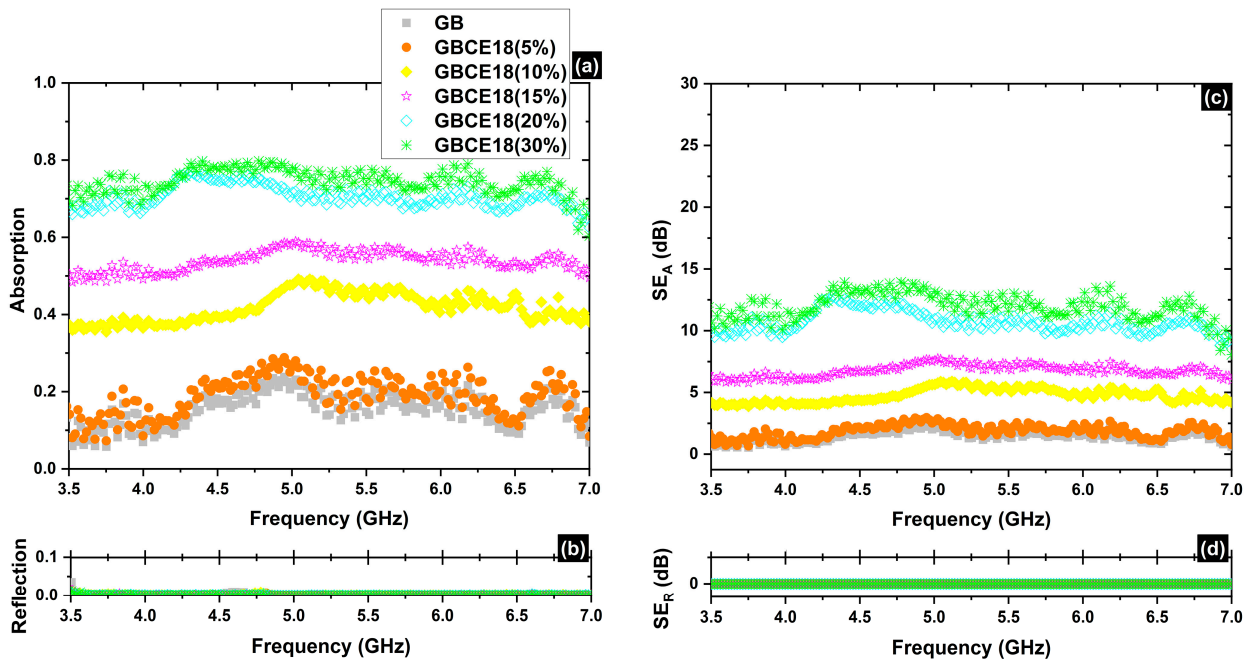


**Figure 11.** Absorption (a) and reflection (b) spectra from 3.5 to 7.0 GHz (C-band) for different gypsum board samples. The electromagnetic interference shielding effect (SE) due to absorption ( $SE_R$ ; (c)) and reflection ( $SE_A$ ; (d)) can also be seen in the frequency range of 3.5–7.0 GHz.

When the loading amount of activated carbon was low, the interconnected electrically conductive network was incomplete, and there was a small difference in electrical conductivity between the gypsum board samples and air, leading to a large impedance match and a large number of electromagnetic waves being transmitted into the samples [67]. Indeed, as one can easily observe in Figure 11c, for RT18HC@AC concentrations from 0.0 to 5% w.t., the  $SE_A$  does not exceed 2.5 dB, while for 10% w.t. up to 30% w.t., the  $SE_A$  varies from 2.5 to 12.5 dB, suggesting the absorption-dominant EMI shielding mechanism of our composite samples, which is in agreement with the properties of other carbon-based composite samples [66].

At this point, it should be noted that an  $SE_T$  of ~15–20 dB is more than sufficient for shielding, e.g., computer devices [64], since an SE of 20 dB corresponds to the blocking of ~99% of incident EM waves.

### 3.2.5. Thermal Performance Measurements

To assess the thermal performance of the test samples, the upper environmental chamber underwent an 8 h heating phase, followed by an 8 h cooling period. Figure 12 illustrates the temperature fluctuations at the inner surfaces (inside the test rooms) of the test samples over time.

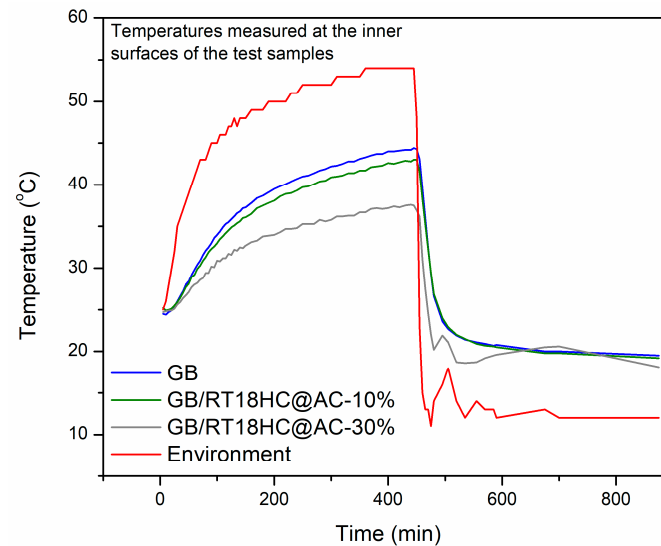


**Figure 12.** Curves from thermal performance measurements for gypsum board samples with 10 and 30% RT18HC@AC loadings in comparison with the reference gypsum board GB.

During the initial stage of the heating process, all test samples exhibited a similar rate of temperature increase. The primary distinction lay in the maximum temperatures recorded. It is evident that the gypsum board with a higher phase change material (PCM) content demonstrated an ability to sustain a lower indoor room temperature for an extended duration. The temperature values of the internal surface (at the plateau of the plots) were 44.4, 43.0, and 37.5 °C for GB, GB/RT18HC@AC-10%, and GB/RT18HC@AC-30%, respectively, while the corresponding temperature values measured at the external surfaces were 46.5, 48.2, and 43.0 °C, respectively. The difference between these values (external-internal) are 2.1, 5.2, and 5.5 °C, respectively.

## 4. Conclusions

In conclusion, the research on enhanced gypsum boards incorporating activated carbon composites and phase change materials for advanced thermal energy storage and electromagnetic interference shielding properties has yielded significant insights and promising outcomes. The encapsulation of RT18HC on AC derived from spent coffee showed no leaching of the PCM component and a high RT18HC loading of ~120.9 wt%. The successful incorporation of RT18HC@AC composites into gypsum boards has demonstrated notable improvements in thermal energy storage capabilities. At the same time, the incorporation of these composite additives into gypsum boards can improve the mechanical properties of the gypsum board. At lower concentrations of RT18HC@AC (up to 10% w.t.), a positive correlation is evident, while at higher concentrations, mechanical degradation becomes apparent, concluding that the optimal content of the additive for gypsum boards is 10% w.t. RTR18HC@AC. The investigation into EMI shielding properties has shown that the RT18HC@-activated carbon composites play crucial roles in attenuating electromagnetic interference. The composite material exhibits promising EMI shielding effectiveness, opening avenues for applications in electronics, telecommunications, and other industries where EMI mitigation is imperative. In addition, the gypsum board with a higher RT18HC content demonstrated an ability to sustain a lower indoor room temperature for an extended

duration. This dual functionality makes enhanced gypsum boards multifaceted solutions for modern construction and technological advancements.

In summary, this research highlights the significance of using enhanced gypsum boards with activated carbon composites and PCMs as a promising solution for addressing the dual challenges of advanced thermal energy storage and electromagnetic interference shielding. The positive outcomes pave the way for practical applications and future innovations in the field of construction materials and technology.

**Supplementary Materials:** The following supporting information can be downloaded at <https://www.mdpi.com/article/10.3390/micro4010005/s1>, Table S1: Density of reference gypsum board and composite gypsum boards; Table S2: Thermal conductivity (k), thermal effusivity (e), and specific heat capacity (Cp) of reference gypsum board and composite boards GB/RT18HC@AC; Table S3. Maximum load (Fmax), absorbed energy (Ea), and percentage increment of Ea (I) for the gypsum boards with varying % w.t. contents of RT18HC@AC additive. Figure S1. Pictures from the custom-made environmental chamber. (a) The chamber during the measurements; (b,c) the internal area of the chamber. Figure S2: Force-displacement plots, obtained from impact resistance tests for gypsum boards with varying % w.t. contents of RT18HC@AC additive.

**Author Contributions:** Conceptualization, M.A.K. and G.K.; methodology, M.A.K., G.K., S.A. and C.E.S.; formal analysis, C.G., K.C.V., M.A.K., G.K., Z.V. and R.I.; investigation, C.G., K.C.V., Z.V. and A.N.; resources, M.A.K., G.K. and A.S.P.; data curation, M.A.K., G.K., S.A., Z.V., C.G., K.C.V., M.B., A.N., A.S.P., C.E.S. and R.I.; writing—original draft preparation, M.B. and M.A.K.; writing—review and editing, M.A.K., G.K. and M.B.; supervision, M.A.K. and G.K.; project administration, M.A.K. and G.K.; funding acquisition, M.A.K. and G.K.; validation, S.A., C.E.S. and R.I. All authors have read and agreed to the published version of the manuscript.

**Funding:** This work was co-financed by the European Union and Greek national funds through the Operational Program Competitiveness, Entrepreneurship and Innovation, under the call RESEARCH—CREATE—INNOVATE (acronym: SEMI-WEB; project code: T2EDK-02073).

**Data Availability Statement:** The data presented in this study are available upon request from the corresponding author.

**Conflicts of Interest:** The authors declare no conflicts of interest.

## References

1. Al-Absi, Z.A.; Mohd Isa, M.H.; Ismail, M. Phase Change Materials (PCMs) and Their Optimum Position in Building Walls. *Sustainability* **2020**, *12*, 1294. [[CrossRef](#)]
2. da Cunha, S.R.L.; de Aguiar, J.L.B. Phase Change Materials and Energy Efficiency of Buildings: A Review of Knowledge. *J. Energy Storage* **2020**, *27*, 101083. [[CrossRef](#)]
3. Zachariah, S.M.; Antony, T.; Grohens, Y.; Thomas, S. From Waste to Wealth: A Critical Review on Advanced Materials for EMI Shielding. *J. Appl. Polym. Sci.* **2022**, *139*, e52974. [[CrossRef](#)]
4. Wu, N.; Hu, Q.; Wei, R.; Mai, X.; Naik, N.; Pan, D.; Guo, Z.; Shi, Z. Review on the Electromagnetic Interference Shielding Properties of Carbon Based Materials and Their Novel Composites: Recent Progress, Challenges and Prospects. *Carbon* **2021**, *176*, 88–105. [[CrossRef](#)]
5. Vaishnav, K.; Lazarus, G.P.; Bansal, S.; Hooda, Y. Review on Thermal Energy Efficiency Using Gypsum Integrated Phase Change Materials in Buildings. In *Proceedings of the Advances in Construction Materials and Sustainable Environment*; Gupta, A.K., Shukla, S.K., Azamathulla, H., Eds.; Springer: Singapore, 2022; pp. 305–319.
6. Sharifi, N.P.; Shaikh, A.A.N.; Sakulich, A.R. Application of Phase Change Materials in Gypsum Boards to Meet Building Energy Conservation Goals. *Energy Build.* **2017**, *138*, 455–467. [[CrossRef](#)]
7. Pasupathy, A.; Velraj, R.; Seeniraj, R.V. Phase Change Material-Based Building Architecture for Thermal Management in Residential and Commercial Establishments. *Renew. Sustain. Energy Rev.* **2008**, *12*, 39–64. [[CrossRef](#)]
8. Yang, A.-S.; Cai, T.-Y.; Su, L.; Li, Y.-S.; He, F.-F.; Zhang, Q.-P.; Zhou, Y.-L.; He, R.; Zhang, K.; Yang, W.-B. Review on Organic Phase Change Materials for Sustainable Energy Storage. *Sustain. Energy Fuels* **2022**, *6*, 5045–5071. [[CrossRef](#)]
9. Rashid, F.L.; Al-Obaidi, M.A.; Dulaimi, A.; Bernardo, L.F.A.; Eleiwi, M.A.; Mahood, H.B.; Hashim, A. A Review of Recent Improvements, Developments, Effects, and Challenges on Using Phase-Change Materials in Concrete for Thermal Energy Storage and Release. *J. Compos. Sci.* **2023**, *7*, 352. [[CrossRef](#)]
10. Liu, X.; Yang, F.; Li, M.; Sun, C.; Wu, Y. Development of Cost-Effective PCM-Carbon Foam Composites for Thermal Energy Storage. *Energy Rep.* **2022**, *8*, 1696–1703. [[CrossRef](#)]

11. Gioti, C.; Karakassides, A.; Asimakopoulos, G.; Baikousi, M.; Salmas, C.E.; Viskadourakis, Z.; Kenanakis, G.; Karakassides, M.A. Multifunctional Carbon-Based Hybrid Foams for Shape-Stabilization of Phase Change Materials, Thermal Energy Storage, and Electromagnetic Interference Shielding Functions. *Micro* **2022**, *2*, 390–409. [[CrossRef](#)]
12. Rathore, P.K.S.; Shukla, S.K. Enhanced Thermophysical Properties of Organic PCM through Shape Stabilization for Thermal Energy Storage in Buildings: A State of the Art Review. *Energy Build.* **2021**, *236*, 110799. [[CrossRef](#)]
13. Abdeali, G.; Bahramian, A.R.; Abdollahi, M. Review on Nanostructure Supporting Material Strategies in Shape-Stabilized Phase Change Materials. *J. Energy Storage* **2020**, *29*, 101299. [[CrossRef](#)]
14. Khadiran, T.; Hussein, M.Z.; Zainal, Z.; Rusli, R. Shape-Stabilised n-Octadecane/Activated Carbon Nanocomposite Phase Change Material for Thermal Energy Storage. *J. Taiwan Inst. Chem. Eng.* **2015**, *55*, 189–197. [[CrossRef](#)]
15. Feng, L.; Zheng, J.; Yang, H.; Guo, Y.; Li, W.; Li, X. Preparation and Characterization of Polyethylene Glycol/Active Carbon Composites as Shape-Stabilized Phase Change Materials. *Sol. Energy Mater. Sol. Cells* **2011**, *95*, 644–650. [[CrossRef](#)]
16. Chen, Z.; Shan, F.; Cao, L.; Fang, G. Synthesis and Thermal Properties of Shape-Stabilized Lauric Acid/Activated Carbon Composites as Phase Change Materials for Thermal Energy Storage. *Sol. Energy Mater. Sol. Cells* **2012**, *102*, 131–136. [[CrossRef](#)]
17. Xia, L.; Zhang, P.; Wang, R.Z. Preparation and Thermal Characterization of Expanded Graphite/Paraffin Composite Phase Change Material. *Carbon* **2010**, *48*, 2538–2548. [[CrossRef](#)]
18. Zhang, Z.; Zhang, N.; Peng, J.; Fang, X.; Gao, X.; Fang, Y. Preparation and Thermal Energy Storage Properties of Paraffin/Expanded Graphite Composite Phase Change Material. *Appl. Energy* **2012**, *91*, 426–431. [[CrossRef](#)]
19. Li, B.; Liu, T.; Hu, L.; Wang, Y.; Nie, S. Facile Preparation and Adjustable Thermal Property of Stearic Acid–Graphene Oxide Composite as Shape-Stabilized Phase Change Material. *Chem. Eng. J.* **2013**, *215–216*, 819–826. [[CrossRef](#)]
20. Mehrali, M.; Latibari, S.T.; Mehrali, M.; Metselaar, H.S.C.; Silakhori, M. Shape-Stabilized Phase Change Materials with High Thermal Conductivity Based on Paraffin/Graphene Oxide Composite. *Energy Convers. Manag.* **2013**, *67*, 275–282. [[CrossRef](#)]
21. Jiang, T.; Zhang, Y.; Olayiwola, S.; Lau, C.; Fan, M.; Ng, K.; Tan, G. Biomass-Derived Porous Carbons Support in Phase Change Materials for Building Energy Efficiency: A Review. *Mater. Today Energy* **2022**, *23*, 100905. [[CrossRef](#)]
22. Li, M.; Mu, B. Effect of Different Dimensional Carbon Materials on the Properties and Application of Phase Change Materials: A Review. *Appl. Energy* **2019**, *242*, 695–715. [[CrossRef](#)]
23. Srinivasaraonai, B.; Singh, L.P.; Sinha, S.; Tyagi, L.; Rawat, A. Studies on the Mechanical Properties and Thermal Behavior of Microencapsulated Eutectic Mixture in Gypsum Composite Board for Thermal Regulation in the Buildings. *J. Build. Eng.* **2020**, *31*, 101400. [[CrossRef](#)]
24. Khadiran, T.; Hussein, M.Z.; Zainal, Z.; Rusli, R. Activated Carbon Derived from Peat Soil as a Framework for the Preparation of Shape-Stabilized Phase Change Material. *Energy* **2015**, *82*, 468–478. [[CrossRef](#)]
25. Hussain, S.I.; Dinesh, R.; Roseline, A.A.; Dhivya, S.; Kalaiselvam, S. Enhanced Thermal Performance and Study the Influence of Sub Cooling on Activated Carbon Dispersed Eutectic PCM for Cold Storage Applications. *Energy Build.* **2017**, *143*, 17–24. [[CrossRef](#)]
26. Chin, C.O.; Yang, X.; Paul, S.C.; Susilawati; Wong, L.S.; Kong, S.Y. Development of Thermal Energy Storage Lightweight Concrete Using Paraffin-Oil Palm Kernel Shell-Activated Carbon Composite. *J. Clean. Prod.* **2020**, *261*, 121227. [[CrossRef](#)]
27. Mert, H.H.; Eslek, A.; Mert, E.H.; Mert, M.S. Preparation and Characterization of Shape-Stable Bio-Based Composite Phase Change Materials for Thermal Energy Storage: Coconut Oil/Activated Carbon from Cherry Stones Doped Composites. *Energy Sources Part Recovery Util. Environ. Eff.* **2022**, *44*, 5381–5397. [[CrossRef](#)]
28. Atinafu, D.G.; Dong, W.; Wang, C.; Wang, G. Synthesis of Porous Carbon from Cotton Using an Mg(OH)<sub>2</sub> Template for Form-Stabilized Phase Change Materials with High Encapsulation Capacity, Transition Enthalpy and Reliability. *J. Mater. Chem. A* **2018**, *6*, 8969–8977. [[CrossRef](#)]
29. Lv, L.; Wang, J.; Ji, M.; Zhang, Y.; Huang, S.; Cen, K.; Zhou, H. Effect of Structural Characteristics and Surface Functional Groups of Biochar on Thermal Properties of Different Organic Phase Change Materials: Dominant Encapsulation Mechanisms. *Renew. Energy* **2022**, *195*, 1238–1252. [[CrossRef](#)]
30. Sarabandi, D.; Roudini, G.; Barahuie, F. Activated Carbon Derived from Pine Cone as a Framework for the Preparation of N-Heptadecane Nanocomposite for Thermal Energy Storage. *J. Energy Storage* **2019**, *24*, 100795. [[CrossRef](#)]
31. Lv, L.; Huang, S.; Zhou, C.; Ma, W. Biochar Activated by Potassium Carbonate to Load Organic Phase Change Material: Better Performance and Environmental Friendliness. *Ind. Crops Prod.* **2023**, *204*, 117184. [[CrossRef](#)]
32. Zeng, S.; Huang, Z.; Jiang, H.; Li, Y. From Waste to Wealth: A Lightweight and Flexible Leather Solid Waste/Polyvinyl Alcohol/Silver Paper for Highly Efficient Electromagnetic Interference Shielding. *ACS Appl. Mater. Interfaces* **2020**, *12*, 52038–52049. [[CrossRef](#)] [[PubMed](#)]
33. Ma, X.; Shen, B.; Zhang, L.; Chen, Z.; Liu, Y.; Zhai, W.; Zheng, W. Novel Straw-Derived Carbon Materials for Electromagnetic Interference Shielding: A Waste-to-Wealth and Sustainable Initiative. *ACS Sustain. Chem. Eng.* **2019**, *7*, 9663–9670. [[CrossRef](#)]
34. Bai, Z.; Zhao, B.; Deng, J.; Ren, Y.; Li, Y.; Wang, R.; Zeng, F.; Guo, X.; Zhang, R. Light-Weight and High-Efficiency Electromagnetic Wave Shielding Properties Based on Waste Straw Porous Carbon. *J. Mater. Sci. Mater. Electron.* **2020**, *31*, 4963–4971. [[CrossRef](#)]
35. Zhang, Y.; Yang, Z.; Yu, Y.; Wen, B.; Liu, Y.; Qiu, M. Tunable Electromagnetic Interference Shielding Ability in a One-Dimensional Bagasse Fiber/Polyaniline Heterostructure. *ACS Appl. Polym. Mater.* **2019**, *1*, 737–745. [[CrossRef](#)]

36. Aslam, M.A.; Ding, W.; ur Rehman, S.; Hassan, A.; Bian, Y.; Liu, Q.; Sheng, Z. Low Cost 3D Bio-Carbon Foams Obtained from Wheat Straw with Broadened Bandwidth Electromagnetic Wave Absorption Performance. *Appl. Surf. Sci.* **2021**, *543*, 148785. [CrossRef]
37. Zhang, Y.; Yang, Z.; Pan, T.; Gao, H.; Guan, H.; Xu, J.; Zhang, Z. Construction of Natural Fiber/Polyaniline Core-Shell Heterostructures with Tunable and Excellent Electromagnetic Shielding Capability via a Facile Secondary Doping Strategy. *Compos. Part Appl. Sci. Manuf.* **2020**, *137*, 105994. [CrossRef]
38. Khasnabis, S.; Jois HS, M.; Bora, P.J.; Ramamurthy, P.C. Comparative Studies on Physical and Chemical Routes for Animal Waste-Derived Activated Carbon for Microwave Absorption in the X-Band. *J. Mater. Sci. Mater. Electron.* **2022**, *33*, 3425–3437. [CrossRef]
39. Borreguero, A.M.; Garrido, I.; Valverde, J.L.; Rodríguez, J.F.; Carmona, M. Development of Smart Gypsum Composites by Incorporating Thermoregulating Microcapsules. *Energy Build.* **2014**, *76*, 631–639. [CrossRef]
40. Yaras, A.; Ustaoglu, A.; Gencel, O.; Sari, A.; Hekimoğlu, G.; Sutcu, M.; Erdogmus, E.; Kaplan, G.; Bayraktar, O.Y. Characteristics, Energy Saving and Carbon Emission Reduction Potential of Gypsum Wallboard Containing Phase Change Material. *J. Energy Storage* **2022**, *55*, 105685. [CrossRef]
41. Serrano, S.; Barreneche, C.; Inés Fernández, A.; Farid, M.M.; Cabeza, L.F. Composite Gypsum Containing Fatty-Ester PCM to Be Used as Constructive System: Thermophysical Characterization of Two Shape-Stabilized Formulations. *Energy Build.* **2015**, *86*, 190–193. [CrossRef]
42. Li, C.; Yu, H.; Song, Y.; Liu, Z. Novel Hybrid Microencapsulated Phase Change Materials Incorporated Wallboard for Year-Long Year Energy Storage in Buildings. *Energy Convers. Manag.* **2019**, *183*, 791–802. [CrossRef]
43. Zhang, Y.; Tao, W.; Wang, K.; Li, D. Analysis of Thermal Properties of Gypsum Materials Incorporated with Microencapsulated Phase Change Materials Based on Silica. *Renew. Energy* **2020**, *149*, 400–408. [CrossRef]
44. Bake, M.; Shukla, A.; Liu, S. Development of Gypsum Plasterboard Embodied with Microencapsulated Phase Change Material for Energy Efficient Buildings. *Mater. Sci. Energy Technol.* **2021**, *4*, 166–176. [CrossRef]
45. Fei, H.; Wang, L.; He, Q.; Du, W.; Gu, Q.; Pan, Y. Preparation and Properties of a Composite Phase Change Energy Storage Gypsum Board Based on Capric Acid-Paraffin/Expanded Graphite. *ACS Omega* **2021**, *6*, 6144–6152. [CrossRef] [PubMed]
46. Chen, C.; Wang, X.; Ma, F.; Wang, Y.; Jiu, S.; Chen, Y. Preparation and Characterization of Modified Activated Carbon-Based Shape Stabilized Eutectic Phase Change Materials for Gypsum Composites Application. *Constr. Build. Mater.* **2023**, *369*, 130551. [CrossRef]
47. Zhang, H.; Xu, Q.; Zhao, Z.; Zhang, J.; Sun, Y.; Sun, L.; Xu, F.; Sawada, Y. Preparation and Thermal Performance of Gypsum Boards Incorporated with Microencapsulated Phase Change Materials for Thermal Regulation. *Sol. Energy Mater. Sol. Cells* **2012**, *102*, 93–102. [CrossRef]
48. Toppi, T.; Mazzarella, L. Gypsum Based Composite Materials with Micro-Encapsulated PCM: Experimental Correlations for Thermal Properties Estimation on the Basis of the Composition. *Energy Build.* **2013**, *57*, 227–236. [CrossRef]
49. Cui, H.; Tang, W.; Qin, Q.; Xing, F.; Liao, W.; Wen, H. Development of Structural-Functional Integrated Energy Storage Concrete with Innovative Macro-Encapsulated PCM by Hollow Steel Ball. *Appl. Energy* **2017**, *185*, 107–118. [CrossRef]
50. Asimakopoulos, G.; Baikousi, M.; Kostas, V.; Papantoniou, M.; Bourlinos, A.B.; Zbořil, R.; Karakassides, M.A.; Salmas, C.E. Nanoporous Activated Carbon Derived via Pyrolysis Process of Spent Coffee: Structural Characterization. Investigation of Its Use for Hexavalent Chromium Removal. *Appl. Sci.* **2020**, *10*, 8812. [CrossRef]
51. Robert, U.W.; Etuk, S.E.; Agbasi, O.E. Modified Water Displacement Method and Its Use for Determination of Bulk Density of Porous Materials. *J. Renew. Energy Mech. REM* **2019**, *2*, 1–16. [CrossRef]
52. Standard Test Method for Measurement of Thermal Effusivity of Fabrics Using a Modified Transient Plane Source (MTPS) Instrument. Available online: <https://www.astm.org/d7984-21.html> (accessed on 18 December 2023).
53. ASTM Standard C90-15; Standard Specification for Loadbearing Concrete Masonry Units. ASTM International: West Conshohocken, PA, USA, 2015.
54. Standard Test Method for Flexural Strength of Concrete (Using Simple Beam with Center-Point Loading). Available online: [https://www.astm.org/c0293\\_c0293m-16.html](https://www.astm.org/c0293_c0293m-16.html) (accessed on 19 December 2023).
55. RT GmbH. *RT18HC*; RT GmbH: Giessen, Germany, 2020.
56. Kim, D.; Jung, J.; Kim, Y.; Lee, M.; Seo, J.; Khan, S.B. Structure and Thermal Properties of Octadecane/Expanded Graphite Composites as Shape-Stabilized Phase Change Materials. *Int. J. Heat Mass Transf.* **2016**, *95*, 735–741. [CrossRef]
57. *Standard EN 13279-1*; Gypsum Binders and Gypsum Plasters. Part 1: Definitions and Requirements. UNE: Madrid, Spain, 2009.
58. López Pedrajas, D.; Borreguero Simón, A.M.; Sáenz, I.G.; Ramos, F.J.; Rodríguez Romero, J.F.; Carmona Franco, M. Thermoregulating Gypsums by Using Nanoencapsulated Phase Change Material Slurry. *J. Therm. Anal. Calorim.* **2022**, *147*, 9959–9973. [CrossRef]
59. Verma, M.; Singh, A.P.; Sambyal, P.; Singh, B.P.; Dhawan, S.K.; Choudhary, V. Barium Ferrite Decorated Reduced Graphene Oxide Nanocomposite for Effective Electromagnetic Interference Shielding. *Phys. Chem. Chem. Phys.* **2014**, *17*, 1610–1618. [CrossRef] [PubMed]
60. Zheng, X.; Tang, J.; Cheng, L.; Yang, H.; Zou, L.; Li, C. Superhydrophobic Hollow Magnetized Fe<sub>3</sub>O<sub>4</sub> Nanospheres/MXene Fabrics for Electromagnetic Interference Shielding. *J. Alloys Compd.* **2023**, *934*, 167964. [CrossRef]

61. Zheng, X.; Cao, W.; Hong, X.; Zou, L.; Liu, Z.; Wang, P.; Li, C. Versatile Electronic Textile Enabled by a Mixed-Dimensional Assembly Strategy. *Small* **2023**, *19*, 2208134. [[CrossRef](#)] [[PubMed](#)]
62. Ameli, A.; Jung, P.U.; Park, C.B. Electrical Properties and Electromagnetic Interference Shielding Effectiveness of Polypropylene/Carbon Fiber Composite Foams. *Carbon* **2013**, *60*, 379–391. [[CrossRef](#)]
63. Al-Saleh, M.H.; Saadeh, W.H.; Sundararaj, U. EMI Shielding Effectiveness of Carbon Based Nanostructured Polymeric Materials: A Comparative Study. *Carbon* **2013**, *60*, 146–156. [[CrossRef](#)]
64. Al-Saleh, M.H.; Gelves, G.A.; Sundararaj, U. Copper Nanowire/Polystyrene Nanocomposites: Lower Percolation Threshold and Higher EMI Shielding. *Compos. Part Appl. Sci. Manuf.* **2011**, *42*, 92–97. [[CrossRef](#)]
65. Viskadourakis, Z.; Vasilopoulos, K.C.; Economou, E.N.; Soukoulis, C.M.; Kenanakis, G. Electromagnetic Shielding Effectiveness of 3D Printed Polymer Composites. *Appl. Phys. Mater. Sci. Process.* **2017**, *123*, 736. [[CrossRef](#)]
66. Zheng, X.; Hu, Q.; Wang, Z.; Nie, W.; Wang, P.; Li, C. Roll-to-Roll Layer-by-Layer Assembly Bark-Shaped Carbon Nanotube/Ti<sub>3</sub>C<sub>2</sub>T<sub>x</sub> MXene Textiles for Wearable Electronics. *J. Colloid Interface Sci.* **2021**, *602*, 680–688. [[CrossRef](#)]
67. Liang, C.; Gu, Z.; Zhang, Y.; Ma, Z.; Qiu, H.; Gu, J. Structural Design Strategies of Polymer Matrix Composites for Electromagnetic Interference Shielding: A Review. *Nano-Micro Lett.* **2021**, *13*, 181. [[CrossRef](#)] [[PubMed](#)]

**Disclaimer/Publisher’s Note:** The statements, opinions and data contained in all publications are solely those of the individual author(s) and contributor(s) and not of MDPI and/or the editor(s). MDPI and/or the editor(s) disclaim responsibility for any injury to people or property resulting from any ideas, methods, instructions or products referred to in the content.